catalysts

MDPI

Article

Optimization of Photocatalytic Degradation of Acid Blue 113 and Acid Red 88 Textile Dyes in a UV-C/TiO_2 Suspension System: Application of Response Surface Methodology (RSM)

Soroosh Mortazavian [1], Ali Saber [2,*] and David E. James [2]

[1] Department of Mechanical Engineering, University of Nevada, Las Vegas, Las Vegas, NV 89154, USA; mortazav@unlv.nevada.edu

[2] Department of Civil and Environmental Engineering and Construction, University of Nevada, Las Vegas, Las Vegas, NV 89154, USA; dave.james@unlv.edu

* Correspondence: sabersic@unlv.nevada.edu; Tel.: +1-702-285-2836

Received: 19 March 2019; Accepted: 8 April 2019; Published: 14 April 2019

Abstract: Textile industries produce copious amounts of colored wastewater some of which are toxic to humans and aquatic biota. This study investigates optimization of a bench-scale UV-C photocatalytic process using a TiO_2 catalyst suspension for degradation of two textile dyes, Acid Blue 113 (AB 113) and Acid Red 88 (AR 88). From preliminary experiments, appropriate ranges for experimental factors including reaction time, solution pH, initial dye concentration and catalyst dose, were determined for each dye. Response surface methodology (RSM) using a cubic IV optimal design was then used to design the experiments and optimize the process. Analysis of variance (ANOVA) was employed to determine significance of experimental factors and their interactions. Results revealed that among the studied factors, solution pH and initial dye concentration had the strongest effects on degradation rates of AB 113 and AR 88, respectively. Least-squares cubic regression models were generated by step-wise elimination of non-significant (p-value > 0.05) terms from the proposed model. Under optimum treatment conditions, removal efficiencies reached 98.7% for AB 113 and 99.6% for AR 88. Kinetic studies showed that a first-order kinetic model could best describe degradation data for both dyes, with degradation rate constants of $k_{1,\,AB\,113} = 0.048$ min^{-1} and $k_{1,\,AR\,88} = 0.059$ min^{-1}.

Keywords: process optimization; response surface methodology; kinetic study; Advanced oxidation processes (AOPs); TiO_2 catalyst; textile wastewater

1. Introduction

Dyes are widely used in several industries such as textile industry, paper, plastics, food, cosmetics and so forth. [1]. The textile industry has large water consumption and thereby, produces copious amounts of colored wastewater. It has been estimated that 1–20% of total dye consumption is lost during the dying process, which is subsequently introduced to the receiving water bodies [2]. Some dyes are carcinogenic and toxic to humans and aquatic biota [3], requiring appropriate treatments. Methods for color removal are generally divided into three main groups: physical, chemical and biological treatments. Physical methods, such as adsorption and screening, only transfer pollutants from one phase to another; therefore post-treatment is necessary for complete removal of contaminants [4]. The toxic nature and complex molecular structures of many dyes limit their biological degradation [5]. Hence, biological methods are usually not able to treat colored wastewaters [6]. In addition, biological methods have a disadvantage of producing large volumes of sludge [7]. Chemical methods, on the

other hand, have demonstrated more promising results [4]. In chemical treatment methods, instead of transferring contaminants from one phase to another, the dyes are converted into harmless substances. Advanced oxidation processes (AOPs) are among the most powerful chemical treatment techniques used for removal of organic compounds. AOPs are characterized by in-situ generation of hydroxyl radicals ($^{\bullet}$OH), which are strongly oxidizing species (oxidative potential +2.8 V) [6]. Hydroxyl radicals unselectively attack organic molecules to degrade them into simpler and less harmful compounds and ultimately, convert them into CO_2, H_2O and mineral acids [4,8,9]. Photocatalytic degradation is an advanced oxidation method in which hydroxyl radicals are generated by irradiating UV light on a semiconductor catalyst [10]. In the past several decades, titanium dioxide (TiO_2) has been proved to be more efficient for the photocatalytic processes than other semiconductors. It is inexpensive, non-toxic, water-insoluble, highly reactive and photochemically stable [6].

In a photocatalytic reaction, when TiO_2 particles are illuminated with a light source having energy greater than its band gap (E_{g,TiO_2} = 3.2 eV), electrons in the valence band promote to the conduction band, creating electron-hole pairs [6,11]. Formation of electron-hole pairs is a fast-reversible reaction. To prevent this, an electron acceptor, which is dissolved in most cases, is necessary to entrap free electrons and reduce the rate of electron-hole recombination [10]. Photogenerated electrons may also react with dye molecules and reduce them [6]. Holes, on the other hand, can react with hydroxide ions (OH^-) or adsorbed H_2O on the catalyst's surface and generate hydroxyl radicals. Finally, dye molecules will react with the formed radicals. This reaction takes place on the surface of the catalyst particles and will continue until complete mineralization of the organic species [10]. The photocatalytic reactions described above can be summarized as [8]:

$$TiO_2 + h\nu \rightarrow e^- + h^+ \quad (1)$$

$$e^- + O_2 \rightarrow O\cdot_2^- \quad (2)$$

$$h^+ + \text{Organic} \rightarrow CO_2 \quad (3)$$

$$h^+ + H_2O \rightarrow \cdot OH + H^+ \quad (4)$$

$$\cdot OH + \text{Organic} \rightarrow CO_2 + H_2O \quad (5)$$

A number of studies have investigated aqueous phase photodegradation of various dyes using TiO_2 catalyst [1,7,9,11–18]. Sohrabi and Ghavami (2008) [1] studied photocatalytic degradation of Direct Red 23 using UV/TiO_2 system. They reported an increase in dye decomposition rate with increasing TiO_2 concentration up to 4.0 g/L; the rate then decreased with further increases in catalyst dose. Juang et al. (2010) [7] investigated photodegradation and mineralization of single and binary Acid Orange 7 (AO7) and Reactive Red 2 (RR2) under UV irradiation in TiO_2 suspensions. Their results showed that after 20 min of UV irradiation with 0.5 g/L TiO_2, complete removals of single AO7 and RR2 were achieved at pH 6.8. Photocatalytic degradation of Amaranth dye was investigated in a UV-C/TiO_2 system by Gupta et al. (2012) [13]. They obtained degradation efficiencies of 17%, 26%, 38% and 64% for UV, UV + H_2O_2, UV + TiO_2 and UV + TiO_2 + H_2O_2 systems, respectively, after 100 min irradiation. Barakat (2011) [9] investigated the removal of Procion® yellow H-EXL dye over TiO_2 suspension and obtained 100% photodegradation efficiency under optimum conditions of pH = 5.0, TiO_2 dose = 1.0 g/L and dye concentration = 10 mg/L. Toor et al. (2006) [14] evaluated the photocatalytic degradation of Direct Yellow 12 in a shallow pond slurry using TiO_2 suspension under irradiation of UV light using black fluorescent lamps lies in UV-A range. After 1.5 h and under optimum conditions (TiO_2 dosage = 2.0 g/L, pH = 4.5 and initial dye concentration = 100 mg/L) complete decolorization was achieved. Khataee et al. (2009) [15] investigated degradation of three azo dyes by UV-A irradiation using immobilized TiO_2 and achieved complete decolorization after 6 h at natural pH and an initial dye concentration of 30 mg/L.

However, to the best knowledge of authors, there are limited numbers of studies [19] which have assessed interaction effects between operational factors in the photocatalytic degradation process of dyes and optimized the process.

There are several classical methods for design and optimization of experiments. For instance, the one-factor-at-a-time method does not consider the interactions among experimental factors [20,21]. The full factorial method, considers interaction effects through a great number of experiments but can be time-consuming and costly in multi-variable systems [20,21]. Response surface methodology (RSM) is a collection of statistical and mathematical methods used for development of a functional relationship between a response of interest and a number of input variables [22]. This method is applied for designing experiments, evaluating the effects of individual operational parameters and their interaction effects and optimizing the parameters, with a significant reduction in the number of experiments [23–25]. Several recent studies have optimized the response of various environmental treatment processes using models based on RSM [19,24–33]. For example, Saber et al. (2014, 2017) [26,27] used RSM to optimize Fenton and photo-Fenton processes for treatment of petroleum refinery effluents, Cifuentes et al. (2017) [34] used RSM for simulation of the ethanol's catalytic steam reforming, Li et al. (2018) [35] used RSM to investigate photocatalytic performance and degradation mechanism of Aspirin by TiO_2, Inger et al. (2019) [36] optimized ammonia oxidation using RSM and Aljuboury et al. (2016) [37] optimized TiO_2/ZnO photodegradation of petroleum refinery wastewaters by using RSM.

The current work, for the first time, optimizes experimental conditions for photocatalytic degradation of two anionic textile dyes, Acid Blue 113 (AB 113) and Acid Red 88 (AR 88), in a TiO_2 suspension system using UV-C irradiation. A simple enclosed bench-scale batch photoreactor was constructed for this study. Mercury vapor UV-C lamps were positioned over a relatively shallow free surface dye solution to provide sufficient light penetration as well as reduce costs of employing quartz tubes to immerse a UV lamp in the solution. In RSM-designed experiments, initial dye concentration, catalyst loading and solution pH were considered as independent parameters. The degradation efficiency of dyes was the target response. Modeling photocatalytic degradation efficiency, examining the influences of several variable parameters on degradation efficiency and their interactions and determining optimum conditions for dye removal were conducted using RSM with a cubic IV optimization method. Kinetic studies were also conducted to evaluate dyes' photodegradation rates under optimum conditions.

2. Results and Discussions

2.1. Stage 1: Preliminary Experiments

Figure 1 shows the effects of different experimental factors on photocatalytic degradation of AB 113 and AR 88 textile dyes in the first stage one-factor-at-a-time preliminary experiments.

Figure 1a shows that increasing TiO_2 dose up to 2.0 g/L and 1.0 g/L, enhanced removal efficiencies of AB 113 and AR 88, respectively. Increases in catalyst dose above these thresholds resulted in decreased removal efficiencies. Even though increase of TiO_2 particles in the solution might provide more active sites for the dye molecules to be adsorbed and degraded, excessive amounts of catalyst particles might aggregate leading to a decreased number of active sites. Excessive TiO_2 doses can also increase the opacity of solution and consequently reduce the penetration of UV light and thus decrease the treatment efficiency [1,38]. These results agreed with the previous studies [1,9,14,38] reporting decreased photocatalytic efficiency when applying TiO_2 dose above an optimum value.

Figure 1b shows that increasing reaction time improved removal percentages for both dyes. A higher overall removal efficiency was observed for AR 88 compared with AB 113 over the entire reaction time. As observed, only 7.4% and 8.7% increases in removal efficiencies were observed after 90 min for AB 113 and AR 88 dyes, respectively, indicating that 90 min was sufficient for most of the dye degradation reactions to occur. Hence, a fixed reaction time of 90 min was considered for both

dyes in the main experiments (i.e., second stage experiments), while other experimental factors (e.g., initial dye concentration, catalyst dose and pH) were optimized using RSM.

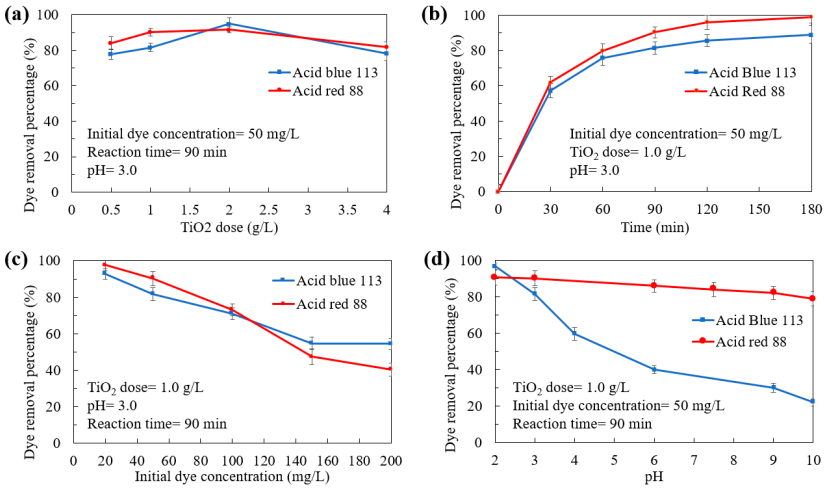

Figure 1. Results of preliminary experiments for photocatalytic degradation of Acid Blue (AB) 113 and Acid Red (AR) 88 textile dyes. Effects of changing (**a**) TiO_2 dose (g/L) (Initial dye concentration = 50 mg/L, pH = 3.0, Reaction time= 90 min), (**b**) reaction time (min) (Initial dye concentration = 50 mg/L, pH = 3.0, TiO_2 dose = 1.0 g/L), (**c**) Initial dye concentration (mg/L) (Reaction time = 90 min, pH = 3.0, TiO_2 dose = 1.0 g/L) and (**d**) pH (Initial dye concentration = 50 mg/L, Reaction time = 90 min, TiO_2 dose = 1.0 g/L). Error bars show standard deviation of duplicate runs.

Figure 1c illustrates that, as expected, increasing dye concentration from 20 mg/L to 200 mg/L decreased removal efficiencies in both dyes (from 97.6% to 40% for AR 88 and from 92.6% to 54.4% for AB 113). This was likely because increasing dye concentration in the solution while maintaining a constant catalyst dose caused the fixed number of catalysis sites to be saturated faster [39]. In addition, increased dye concentration probably decreased the light transmittance in the solution. Decreased UV penetration can reduce the activation rate of TiO_2 particles and hinder the generation of $^{\bullet}OH$ radicals, resulting in decreased photocatalytic degradation efficiencies for both dyes [39].

Figure 1d represents the effects of changing pH from 2.0 to 10.0 on removal efficiencies of AB 113 and AR 88. For AB 113, increasing pH from 2.0 to 6.0 caused a marked decrease in removal efficiency from 96.7% to 40.3% (56.4% decrease). Further increasing pH above 6.0 up to 9.0 decreased efficiency by only an additional 18%. For AR 88, increasing solution pH from 2 to 10 only resulted in 11.8% decrease in degradation efficiency. Detailed discussion about the effects of solution pH on each of dyes and possible interactions with other factors are presented next in Section 2.2.

In order to investigate the sole contribution of adsorption in removal of dyes from the aqueous solutions, experiments were conducted under dark conditions (i.e., without UV-C radiation) for both AB 113 and AR 88 dyes. After 90 min reaction under dark conditions in the closed photoreactor under the fixed experimental conditions of TiO_2 dose = 1.0 g/L, initial dye concentration = 50 mg/L and pH = 3.0, concentrations of both AB 113 and AR 88 remained unchanged when the reacted samples were analyzed by the UV-VIS spectrophotometer. This showed that adsorption onto TiO_2 particles did not by itself have a significant role in dye removal, demonstrating that the observed removal of dyes in the UV-C/TiO_2 system were due to photocatalytic process.

2.2. Stage 2: Process Optimization

2.2.1. Response Surface Plots, Fitted Models and ANOVA

Figures 2 and 3 show the results obtained from the 30 experimental runs (i.e., stage 2) for AB 113 and AR 88, respectively, after 90 min reaction time. Analysis of variance (ANOVA) for AB 113 and AR

88 are presented in Tables 1 and 2, respectively. Significance of the model terms was evaluated based on computed F-statistic values and their associated *p*-values. Least-squares cubic regression models were generated by eliminating non-significant terms (*p*-value > 0.05). Reduced cubic models for AB 113 and AR 88 are expressed in the Equations (6) and (7), respectively.

$$\text{AB 113 Removal (\%)} = 76.75 - 21.30A - 17.41B - 12.47C + 2.28AB - 2.26AC - 8.06A^2 - 11.57B^2 - 5.14A^2C - 4.44AB^2 + 5.23AC^2 + 16.52B^3 \quad (6)$$

$$\text{AR 88 removal (\%)} = 74.21 - 2.00A - 7.67B - 19.61C - 2.03AC - 1.25BC - 11.18B^2 - 1.63ABC + 3.57AB^2 - 3.99AC^2 - 3.30B^2C - 4.44A^3 + 7.18B^3 - 3.95C^3 \quad (7)$$

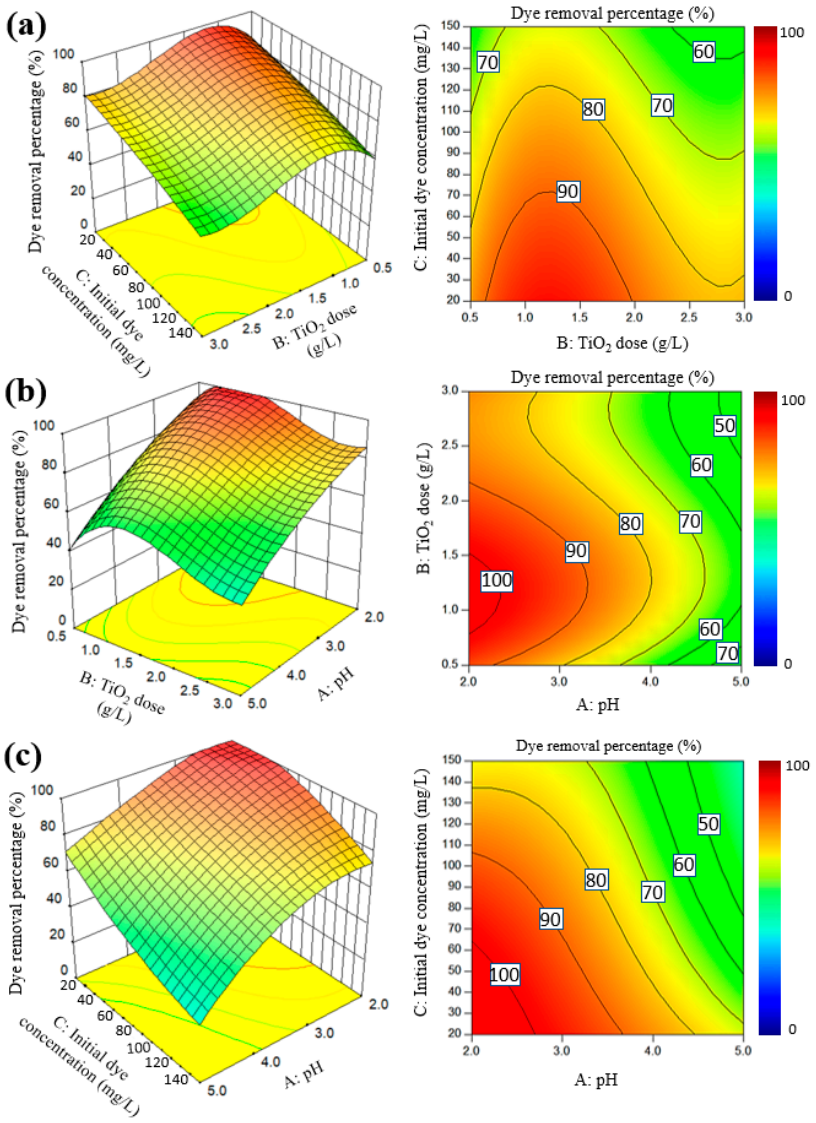

Figure 2. Response surface and contour plots for photocatalytic degradation of AB 113 as a function of (**a**) C: initial dye concentration (mg/L) and B: TiO_2 dose (g/L) (pH = 3.0, reaction time = 90 min), (**b**) A: pH and B: TiO_2 dose (g/L) (initial dye concentration = 50 mg/L, reaction time = 90 min) and (**c**) A: pH and C: initial dye concentration (mg/L) (TiO_2 dose = 1.0 g/L, reaction time = 90 min).

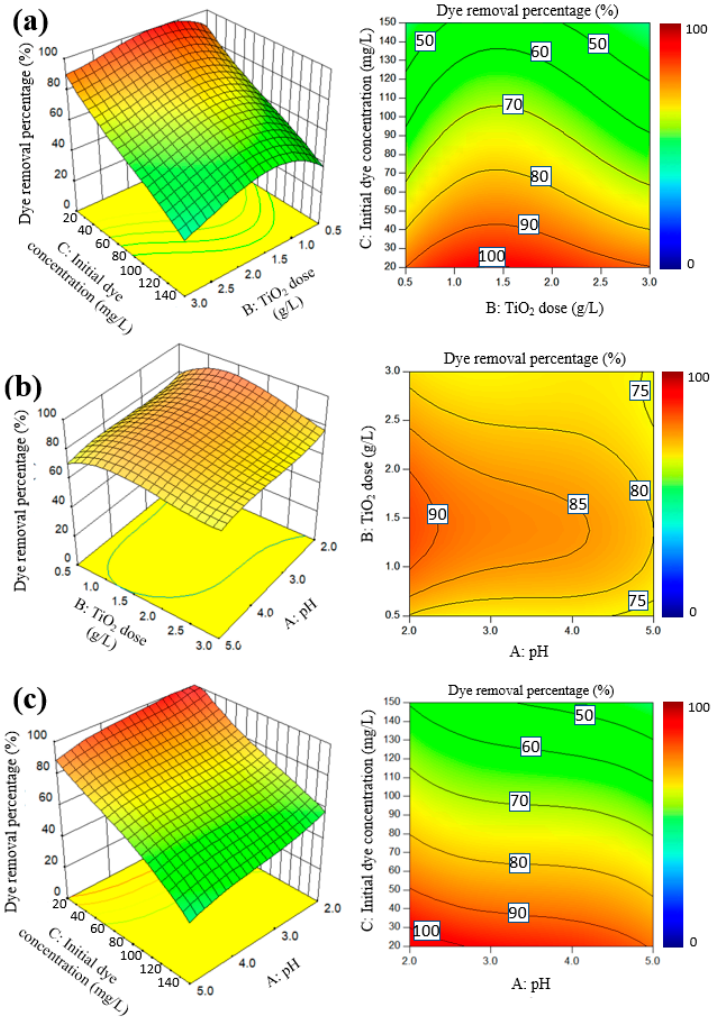

Figure 3. Response surface and contour plots for photocatalytic degradation efficiency of AR 88 as a function of (**a**) C: initial dye concentration (mg/L) and B: TiO_2 dose (g/L) (pH = 3.0, reaction time = 90 min), (**b**) A: pH and B: TiO_2 dose (g/L) (initial dye concentration = 50 mg/L, reaction time = 90 min) and (**c**) A: pH and C: initial dye concentration (mg/L) (TiO_2 dose = 1.0 g/L, reaction time = 90 min).

Table 1. Analysis of variance for modified cubic model obtained for photocatalytic degradation of AB 113 in the UV-C/TiO_2 system.

Source	F-Statistic Value	*p*-Value
Model	86.33	<0.0001
A-pH	129.56	<0.0001
B-TiO_2 dose (g/L)	18.05	0.0005
C-Initial dye concentration (mg/L)	44.81	<0.0001
AB	4.11	0.0578
AC	4.58	0.0462
A^2	20.69	0.0002
B^2	50.53	<0.0001
A^2C	5.13	0.0360
AB^2	4.56	0.0467
AC^2	5.87	0.0261
B^3	14.68	0.0012
Lack of Fit	0.51	0.8499

Table 2. Analysis of variance for modified cubic model obtained for photocatalytic degradation of AR 88 in the UV-C/TiO_2 system.

Source	F-Statistic Value	*p*-Value
Model	217.009	<0.0001
A-pH	0.773	0.392
B-TiO_2 dose (g/L)	14.338	0.0016
C-Initial dye concentration (mg/L)	92.905	<0.0001
AC	9.611	0.0069
BC	3.301	0.088
B^2	90.316	<0.0001
ABC	4.961	0.0406
AB^2	6.835	0.0188
AC^2	6.427	0.0221
B^2C	5.822	0.0282
A^3	3.379	0.0847
B^3	10.334	0.0054
C^3	3.466	0.0811
Lack of Fit	1.312	0.4046

Figure 2 shows that removal efficiencies greater than 90% for AB 113 occurred for conditions of pH between 2.0 and 3.0, TiO_2 dose of 0.7 to 2.0 g/L and dye concentration of 20 to 65 mg/L.

For AR 88, Figure 3 shows that removal efficiencies greater than 90% occurred for conditions of pH between 2.0 and 4.5, TiO_2 dose of 1.0 to 2.0 g/L and dye concentration between 20 and 30 mg/L.

As observed from Figure 2 and Equation (6), AB 113 removal efficiency decreased with increasing pH (term *A*) and initial dye concentration (term *C*), which is consistent with preliminary experiments. pH could affect the speciation of dye molecules and consequently, the electrostatic force between catalysts particles and dye molecules. Since chemical reactions associated with photocatalytic degradation take place on the surface of the catalyst particles [10,38], adsorption of the contaminants' molecules onto catalyst surface is an essential step for efficient photocatalytic degradation [40].

The point of zero charge (zpc) for TiO_2 Degussa P 25 is 6.5 [41]. Hence, the TiO_2 surface was positively charged at pH < 6.5 and negatively charged at pH > 6.5. On the other hand, AB 113 is a disulfonate acid dye (having two sulfonated ($-SO_3^-$) groups) with an acid dissociation constant (pKa) of 0.5 [38]. Therefore, AB 113 tended to be negatively charged at pH > 0.5. The increased density of positive charges on the surface of TiO_2 particles under acidic conditions was likely to be favorable for adsorbing AB 113 [42] and consequently improved photodegradation efficiency. The cubic regression model also showed that there were interaction effects between these two factors (i.e., *A* for pH and *C* for dye concentration) due to presence of the statistically-significant terms *AC*, A^2C and AC^2 in the equation. These significant interactions indicated that changing pH affected the speciation and ionization state of AB 113 dye molecules as well as TiO_2 particles' surface charge [43].

Effects of catalyst dose (term *B*) on AB 113 dye degradation were also consistent with preliminary experiments, as well as studies reported in the literature [1,9,14], which is improving removal efficiency by increasing TiO_2 dose to an optimum point and then reducing the efficiency at greater values. Statistically significant (p-value < 0.05) interactions between the catalyst dose (term *B*) and the solution pH (term *A*) were also observed in ANOVA results. These interactions could be due to the effect of pH on the surface charge of TiO_2, affecting the adsorption of dye molecules on its surface. Since the reaction between hydroxide ions in the solution and holes on the surface of TiO_2 particles could generate hydroxyl radicals, an alkaline environment could be favorable for hydroxyl radicals' generation. However, the electrostatic repulsion between the negatively charged surface of TiO_2 and OH^- anions in an alkaline environment would hinder the formation of hydroxyl radicals leading to a reduced degradation efficiency [44]. Venkatachalam et al. [45] reported that an acidic environment is beneficial for photocatalytic degradation by TiO_2, since it minimizes electron-holes recombination and enhances $^{\bullet}OH$ production. In addition, TiO_2 particles agglomerate in alkaline conditions, leading to a reduced

exposed surface area to the energy source (UV-C light) [46]. This could be another reason for the decreased removal efficiency of both dyes at higher pH values.

Mohammadzadeh et al. (2015) [38] investigated the photodegradation of AB 113 using ZnO-Ag catalyst under UV illumination. They reported that although there is a stronger electrostatic attraction force between ZnO-Ag and AB 113 at 0.5 < pH < 9.0, which is favorable for photocatalytic degradation reactions, since the catalyst dissolves at pH < 3.0, the overall decolorization was enhanced at higher pH values. Ma et al. (2011) [47] studied photooxidation of three azo dyes including AB 113 using TiO_2/H_2O_2 under vacuum ultraviolet (VUV, λ < 190 nm) irradiation. Consistent with the results of the present study, they found that lower pH values (in their experimental range of 3.0 < pH < 9.0) enhanced AB 113 photodegradation.

Figure 3 shows that AR 88 removal efficiencies exceeding 90% occurred for dye concentrations between 20 and 53 mg/L and TiO_2 doses between 1.0 and 2.0 g/L. In the studied range, pH (term *A*) was not found to be a significant factor in AR 88 removal efficiency. Increasing initial AR 88 dye concentration (term *C*) reduced its degradation efficiency. Table 2 and Equation (7) indicate high interactions between all three factors (*AC*, *BC*, *ABC*, AB^2, AC^2 and B^2C). Presence of interaction terms between *A* and *C* (i.e., pH and initial dye concentration) in the regression model suggested that these two factors were not completely independent. Hence, it could be inferred that changing pH in a wider range probably would show more intense effects on the response. This could also be explained by the electrostatic repulsion between negatively charged surface of TiO_2 particles in alkaline environment and negatively charged sulfonic groups ($R\text{-}SO_3^-$) present in structure of AR 88 [3,43]. Therefore, increased negative surface charge of TiO_2 particles due to increased pH could have hindered adsorption of AR 88 onto catalyst surface and consequently, reduced the removal efficiency. However, a pK_a of 10.7 for AR 88 [48] suggests that AR 88 was not highly ionized in the pH range used in this study. Thus, pH effects on degradation of AR 88 were not very significant. Similar to AB 113, changing TiO_2 dose (term *B*) showed an optimum point for AR 88 photodegradation beyond which increasing catalyst dose reduced removal efficiency. For AR 88, the pH parameter (term *A*) was kept in the model because of the significant interaction effects between pH and other factors (i.e., *AC*, AC^2, *ABC*, AB^2).

The obtained models' *p*-values of < 0.0001 demonstrated significance of cubic models for both dyes. High lack-of-fit *p*-values of 0.8499 and 0.4046 for AB 113 and AR 88, respectively, confirmed that both reduced cubic models were statistically significant. High calculated F-statistic values and correspondingly low associated *p*-values for each retained parameter (Tables 1 and 2) indicated highly significant effects of each retained specific parameter or combination of parameters on removal efficiency. The potency of experimental variables on changing removal percentages could be graded as pH > initial dye concentration > TiO_2 dose for AB 113 and initial dye concentration > TiO_2 dose > pH for AR 88. In addition, interaction between pH and the second power of initial dye concentration for AB 113 (AC^2) was found to be the most significant interaction, while for AR 88 the interaction between pH and initial dye concentration for (*AC*) was the most significant interaction (See Figure S1).

A summary of the fitted models' statistical characteristics for two studied dyes, as well as for the cubic models before modification is shown in Table 3.

Values of R^2_{adj} of 0.9700 for AB 113 and 0.9898 for AR 88 (Table 3) indicate that both reduced models could describe a very large portion of the variance in the design space. Table 3 shows coefficients of variation (standard deviation/mean) of 5.88% and 3.47% for AB 113 and AR 88, respectively, meaning that standard deviations were 5.88% and 3.47% of the mean, respectively.

Table 3. Summary of fitted models' characteristics for photocatalytic degradation of AB 113 and AR 88 textile dyes in UV-C/TiO_2 system, before and after removing insignificant terms.

Item	AB 113		AR 88	
	Initial Cubic Model	Reduced Cubic Model	Initial Cubic Model	Reduced Cubic Model
Standard deviation	3.90	3.78	2.35	2.27
Mean	64.24	64.24	65.35	65.35
Coefficient of variation, %	6.06	5.88	3.60	3.47
PRESS	1205.01	664	1780.39	265.73
R^2	0.9890	0.9814	0.9962	0.994
R^2_{adj}	0.9682	0.9700	0.9890	0.990
Adequate precision	26.392	34.834	33.969	42.061

Adequate precision was obtained 34.834 and 42.061 for AB 113 and AR 88, respectively. Values greater than 4 for this factor are desirable. High values denote an adequate signal and show that the model can navigate the design space [23]. Comparing values before and after models' modification, it is observed in Table 3 that the modifications enhanced the signal-to-noise ratio for both dyes, reflected as increased adequate precision values.

For a specific model, a lower value for the Predicted Residual Error Sum of Squares (PRESS, see Equation (13) in Section 3.4) is favorable, showing that the model is not overly sensitive to any single data point [49]. Table 3 shows that PRESS values decreased by 81.5% and 567% after modification of AB 113 and AR 88 models, respectively, indicating that the cubic models were improved by removing statistically insignificant data points.

2.2.2. Optimization

In order to verify the accuracy of the reduced cubic models in predicting optimum treatment condition, a third round of experiments was carried out under optimum conditions. Predicted optimum operating conditions and removal efficiencies as well as the obtained experimental results are shown in Table 4. Removal efficiencies of 98.7% and 99.6% under optimum conditions were achieved for AB 113 and AR 88 dyes, respectively; values reasonably close to 100% removal efficiencies predicted by the reduced cubic models.

Table 4. Optimum conditions for photocatalytic degradation of AB 113 and AR 88 dyes in UV-C/TiO_2 suspension system.

	pH	Initial Dye Concentration (mg/L)	TiO_2 Dose (g/L)	Predicted Removal Efficiency (%)	Achieved Removal Efficiency (%)
AB 113	2.21	43.13	0.98	100%	98.7%
AR 88	2.36	22.40	1.22	100%	99.6%

Regarding the practical applications of the optimized conditions, it should be noted that although highly acidic conditions—causing high operational costs—were proposed for the complete degradation of both AB 113 and AR 88, Figures 2 and 3 illustrate that high removal efficiencies could be achieved in a wider range of operating conditions. For example, having an initial dye concentration of 50 mg/L and a reaction time of 90 min, removal efficiencies of almost >80% could be achieved with pH increased to 4.0 and 5.0 for AB 113 and AR 88, respectively.

2.3. Stage 3: Kinetics of Photocatalytic Degradation

In order to evaluate photocatalytic degradation rates of AB 113 and AR 88, kinetic studies were performed for each dye under the optimum experimental conditions. Results are shown in Figure 4

and reaction rate constants and model characteristics associated with fitted kinetic models are shown in Table 5.

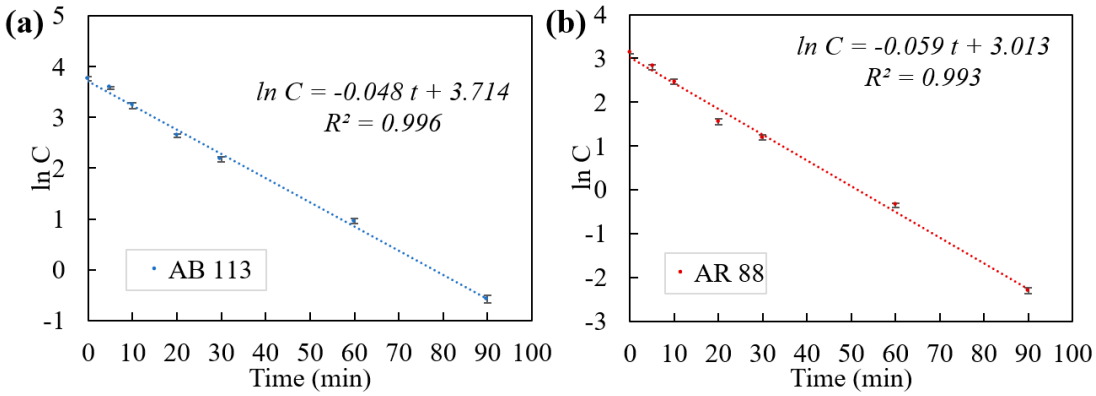

Figure 4. First-order kinetic models for photocatalytic degradation of (**a**) AB 113 and (**b**) AR 88 dyes in UV/TiO_2 suspension system under optimized conditions for each dye (AB 113: initial dye concentration = 43.13 mg/L, reaction time = 90 min, TiO_2 dose = 0.98 g/L, pH = 2.2; AR 88: initial dye concentration = 22.40 mg/L, reaction time = 90 min, TiO_2 dose = 1.22 g/L, pH = 2.4). Error bars show standard deviation.

Table 5. Characteristics of First order kinetic models for photocatalytic degradation of AB 113 and AR 88 in a UV-C/TiO_2 suspension system.

	k_1 (min^{-1})	*p*-Value for k_1	$C_{o,\,model}$	*p*-Value for ln C_o	R^2	*RMSE* (mg/L)
AB 113	0.048	2.13×10^{-7}	41	1.13×10^{-8}	0.996	1.72
AR 88	0.059	8.60×10^{-7}	20.4	3.70×10^{-7}	0.993	1.12

High coefficients of determination ($R^2_{AB\ 113}$ = 0.996 $R^2_{AR\ 88}$ = 0.993) and low root mean square error (*RMSE*) values ($RMSE_{C,\,AB\ 113}$ = 1.72 and $RMSE_{C,\,AR\ 88}$ = 1.12) between the first order kinetic models and experimental values shown in Table 5 demonstrated that first-order kinetic models were appropriate for observed dye degradation under optimum conditions.

AR 88 showed a higher degradation rate compared to AB 113 ($k_{1,\,AR\ 88}$ = 0.059 min^{-1} with a *p*-value of 8.60×10^{-7} compared to $k_{1,\,AB\ 113}$ = 0.048 min^{-1} with a p-value of 2.13×10^{-7}) under optimum conditions. This is consistent with the preliminary results shown in Figure 1b indicating a higher removal percentage for AR 88 compared to AB 113 at all reaction times.

Ma et al. (2011) [47] reported a pseudo-first order rate constant of k = 0.2469 min^{-1} at pH = 3.0 as the highest degradation rate for AB 113 with an initial dye concentration of 0.0523 mM in the studied pH range of 3.0 to 11.0, using a VUV/TiO_2 system, with the VUV lamp immersed in the dye solution and TiO_2 dose of 0.5 g/L. After 60 min, 60% of AB 113 was decomposed. The higher reaction rate obtained by Ma et al. (2011) [47] compared to the present study could be due to the application of VUV, with a lower wavelength and thus higher energy compared to UV-C, which potentially enhance the excitation of TiO_2 particles. In addition, immersing the VUV lamp inside the dye solution using a quartz tube also provides a better exposure of catalyst particles to the energy source. The present study proposed a more economical approach by using a higher wavelength UV-C (meaning a lower energy, primary emission band 254 nm) source and eliminating the use of quartz-tube through direct radiation of UV on the solution surface. Mohammadzadeh et al. (2015) [38] obtained a pseudo-first-order rate constant of 0.007 min^{-1} for AB 113 photodegradation in a ZnO-Ag/UV system with an immersed UV lamp, under the conditions of initial dye concentration = 40 mg/L, catalyst dose = 0.15 g/L and optimum pH = 8.0. After 90 min, almost 50% of AB 113 degraded. Their lower degradation rate compared to the present study might be due to the application of a different catalyst at a lower dose.

Anandan et al. (2008) [11] studied the photocatalytic degradation of AR 88 using Ag-loaded TiO_2 particles (Ag/TiO_2) under visible light and compared the photodegradation rates with using unloaded

TiO_2. They obtained first-order rate constants of about 0.006 min^{-1} and 0.008 min^{-1} for TiO_2 and Ag/TiO_2, respectively, using an initial AR 88 concentration of 0.034 mg/L, a TiO_2 dose of 0.6 g/L, with no pH adjustments. After 425 min, 55% TOC removal was observed using Ag/TiO_2. Konyar et al. (2017) [50] studied photocatalytic degradation of AR 88 using sintered-reticulated ZnO catalyst under UV-A and UV-C radiations, in a quartz tube reactor surrounded by a cylindrical light assembly. They obtained pseudo-first order rate constants of about 0.007 min^{-1} and 0.009 min^{-1} for photodegradation under UV-A and UV-C radiations, respectively, having initial AR 88 concentration of 50 mg/L and catalyst dose of 40 g/L, without pH adjustment. After 180 min, 60% and 80% color removal percentages were obtained under UV-A and UV-C radiation, respectively.

As shown in Figure 5, AB 113 is a diazo naphthyl dye and AR 88 is a mono-azo naphthyl dye, having conjugated chromophores responsible for their color. When TiO_2 is added to the dye solutions, AB 113 and AR 88 molecules are adsorbed mainly through their sulfonate groups [51]. The main degradation pathway proposed by previous researchers studying photodegradation of naphthyl azo dyes in AOP systems [51,52] is the attack of hydroxyl radicals to the naphthalene ring, forming a hydroxylated naphthyl azo dye which is subsequently cleaved. Additionally, hydroxyl radicals attack the aromatic rings with azo groups resulting in azo bond cleavage. Both these reactions result in chromophoric group destruction [52]. Mohammadzadeh et al. (2015) [38] investigated degradation pathway and reaction byproducts for AB 113 photodegradation using a ZnO-Ag nanophotocatalyst under UV radiation. They showed that cleavage of azo bond during a 90 min photocatalysis reaction resulted in the formation of 4-diazenyl-1-naphthylamine, 1-naphthyldiazene or 5-diazenyl-1-naphthol intermediate compounds, which were gradually converted to CO_2 and H_2O [38]. Madhavan et al. (2010) [53] proposed a pathway for the TiO_2 mediated photocatalytic degradation of AR 88 by investigating reaction intermediates using a mass spectrometer and showed formation of hydroxyamino naphthol (4) and 4-aminonaphthalene sulfonic acid (5) as the intermediate products. In the proposed pathway, they showed that AR 88 photocatalytic degradation was mainly due to the hydroxyl radical attack to the aromatic rings [53]. It is expected that the mechanism of hydroxyl radicals attack to AB 113 and AR 88 molecules in the UV-C/TiO_2 system to be similar to the mechanisms proposed by Mohammadzadeh et al. (2015) [38] and Madhavan et al. (2010) [53], consisting of cleavage of azo bonds.

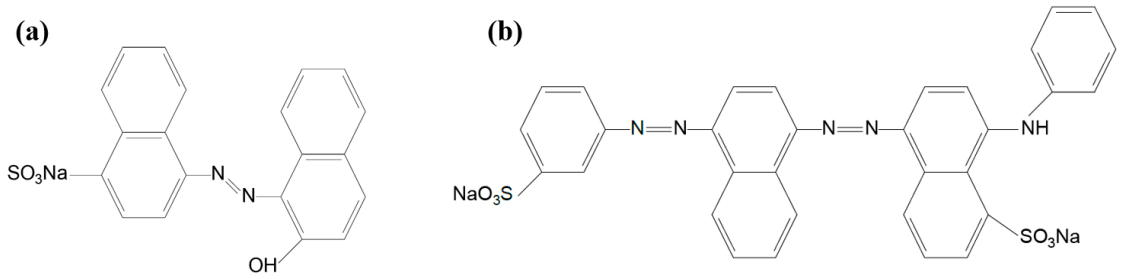

Figure 5. Molecular structure of (**a**) Acid Red 88, pKa = 10.7 and (**b**) Acid Blue 113, pKa = 0.5.

3. Materials and Methods

3.1. Materials and Equipment

Acid Red 88 (AR 88) (also known as Fast Red A or 2-Naphthol Red; CAS number 1658-56-6; molecular formula $C_{20}H_{13}N_2NaO_4S$; molecular weight 400.38 g/mole) and Acid Blue 113 (AB113) (Fast Navy Blue 5R; CAS number 3351-05-1; molecular formula $C_{32}H_{21}N_5Na_2O_6S_2$; molecular weight 681.65 g/mole) were purchased from Sigma-Aldrich (St. Louis, MO, USA) (dye content 75%). Both of these dyes are common azo acid dyes, usually applied for wool, nylon, rayon and polyester dyeing [54]. Acid dyes are negatively charged dyes [55], which are protonated in pH values below their acid dissociation constant (pKa). The chemical structure of AR 88 and AB 113 are shown in Figure 5. Titanium dioxide (TiO_2) Degussa P25 with an average particle size of 30 nm [14] and surface area of 57 m^2/g [11] was purchased from Merck (Kenilworth, NJ, USA) (reagent grade) and used as received.

Solutions of 1 M, 0.1 M and 0.01 M of HCl and NaOH were used to adjust solution pH to pre-determined values before initialization of photocatalytic process. Standard buffer solutions of pH of 4.0 and 7.0 were used to calibrate the pH meter (Jenway, staffordshire, UK) 3045 Ion Analyzer pH meter with a Sentek (Stepney, Australia) single-junction, glass body combination electrode filled with AgCl). To separate TiO_2 particles from treated solutions, 8 mL of treated dye solutions were poured in 15 mL-polypropylene centrifuge tubes (17 mm × 120 mm). A Sigma (St. Louis, MO, USA) 201 centrifuge machine was used at 4000× *g* rpm for 40 min to separate particles. The supernatant was then decanted and used for analysis. Laboratory scales [Sartorius-AC 121S-00MS (Göttingen, Germany) and Rad Wag-WTB 3000 (Radom, Poland)] with the resolution of 0.001 g were used to measure the mass of dyes and TiO_2 particles. All the experiments were carried out using DI water (with an electrical resistivity of 1 MOhm/cm at 25 °C). A Rayleigh (Beijing, China) UV1601 UV/VIS spectrophotometer was calibrated against standard dye solution concentrations and used to measure the dye concentration.

3.2. Photoreactor

Photocatalytic degradation experiments were conducted in a batch reactor, shown schematically in Figure 6. The reactor setup consisted of two UV-C lamps [each lamp: Philips (Somerset, NJ, USA) TUV G30T8 25PK; 30 W, 0.37 A, 102 V; primary emission 253.7 nm, UV-C radiation 12 W, 10% depreciation during 9000 h; 90 cm length, 28 mm diameter], two 4.5-volt rotary agitators, an aeration pump [Hailea (Guangdong, China) ACO 5505, 6 Watt, air output = 5.5 L/min] with two output tubes and two cylindrical dishes (Schott, Germany) for holding dye solutions, with an inside diameter of 13 cm, height of 7.5 cm and bottom thickness of 5 mm. UV lamps were placed on two concrete columns with a height of 25 cm on the top of dye solutions' containers. Distance from the UV lamps to the surface of dye solutions was 20.7 cm. To ensure a homogenous stirring of catalyst particles in dye solutions during the photocatalytic process, samples were agitated at 150 rpm using rotary agitators. Aeration pump tubes were placed in sample containers to supply the oxygen demand for photocatalytic reaction with the oxygen flow rate of 3.9×10^{-2} mole/min, as well as to achieve a uniform suspension of TiO_2 particles in the aqueous solutions. To prevent UV-C radiation leakage, the reactor setup was covered with a cardboard box of 30 cm × 40 cm × 110 cm dimensions. The internal surface of the box was completely covered with aluminum foil to prevent escape of UV radiation. By reflecting the radiation toward the samples, the removal efficiency would likely be enhanced.

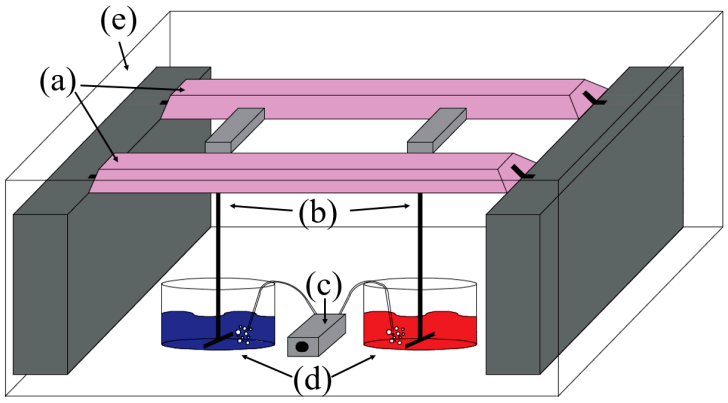

Figure 6. Schematic of the UV-C/TiO_2 photoreactor set up: (**a**) UV-C lamps, (**b**) agitators, (**c**) aeration pump, (**d**) sample containers (**e**) photoreactor cover.

3.3. Experimental Procedure and Measurements

Fresh dye solutions were prepared by adding appropriate amounts of dye powder and DI water in 500-mL volumetric flasks. The solutions were agitated for 10 min on a rotary shaker to obtain a homogenous dye solution and then poured into the cylindrical reaction dishes. Dye solution pH was

adjusted to the predetermined levels and the predetermined masses of TiO_2 powder were added to the solutions. The suspensions were immediately placed in the photoreactor and the mechanical agitators and air pump were simultaneously turned on sand worked in the dark for 5 min. After 5 min, the two UV lamps were turned on to initiate the photocatalytic reactions. Reaction time was measured from the beginning of UV irradiation. All the experiments were carried out at room temperature (23 ± 0.1 °C). To monitor the effectiveness of the process, light absorbance of the samples was measured by the UV-VIS spectrophotometer at characteristic wavelengths of 505 nm and 565 nm for AR 88 and AB 113, respectively [16,56]. Dye concentrations in treated samples were determined from measured light extinction based on Beer–Lambert's law as expressed below:

$$\log_{10}(I/I_o) = A \tag{8}$$

$$A = \varepsilon \cdot L \cdot C \tag{9}$$

where I_o/I is the ratio of incident light to transmitted light, A is light absorbance, ε is the molar absorption coefficient (L mg^{-1} cm^{-1}), L (cm) is the length of solution that light passes through, which is equal to cell thickness used in spectrophotometer and C is the concentration of solution (mg/L) [57]. For dye concentrations ranging between 20 to 200 mg L^{-1}, the light absorption versus dye concentration plots at the peak of each dye's absorption spectrum were linear for both dyes (Figure S2). The extinction coefficient (ε) showed values of 0.20 L mg^{-1} cm^{-1} for AR 88 and 0.21 L mg^{-1} cm^{-1} for AB 113 (Figure S1).

Degradation efficiency, R (%), was calculated using Equation (10):

$$R(\%) = \frac{C_i - C_f}{C_i} \times 100 \tag{10}$$

where C_i and C_f are initial and final dye concentrations (mg/L).

3.4. Statistical Analysis

Apart from R^2 and standard deviation as the two well-known statistical analysis measures, analysis of variance (ANOVA) uses other standard factors to evaluate significance of a fitted regression model to a data set. These factors include coefficient of variation, adequate precision and predicted residual error sum of squares.

Coefficient of variation is the standard deviations which is expressed as the mean percentage:

$$\text{Coefficient of variation } (\%) = \frac{\text{Standard deviation}}{\text{mean}} \times 100 \tag{11}$$

Adequate precision is an indicator for measuring signal to noise ratio of the model, which is calculated as:

$$\text{Adequate precision} = \frac{\text{maximum predicted response} - \text{minimum predicted response}}{\text{Average standard deviation of all predicted response}} \tag{12}$$

Predicted residual error sum of squares (PRESS) is a measure between the fitted values and observed values. From a fitted model, each observation from the data set is removed, the model is refitted and the predicted value at that excluded point is calculated. The PRESS is calculated as: [50]

$$PRESS = \sum_{i=1}^{n} (y_i - \hat{y}_{-i})^2 \tag{13}$$

where n is the number of data points, y_i is the outcome of ith data point and the $\hat{y}_{-i}$ is the prediction of ith data point from the refitted model excluded ith data [58].

The F-test in ANOVA investigates if the variance between the means of two populations are significantly different. The F-statistic is the ratio of the "between-group variability" to the "within-group variability", or:

$$F = \frac{variation\ between\ sample\ means}{variation\ within\ the\ samples} \quad (14)$$

The *p*-value tests the null hypothesis which expresses that data from all groups are from populations with equal means. In other words, *p*-value determines that if all the populations really have the same mean, what is the chance that random sampling would result in the means as far apart as observed. The *p*-value is computed from a comparison of the computed F-statistic to the critical value of the F-statistic for the given number of degrees of freedom.

If the null hypothesis of no significant difference between sample manes is true, the F-statistic is expected to be close to 1. A large F-statistic means that the variation among the group means is more than is expected to occur by chance. Therefore, a large F-statistic, if it exceeds the critical F-statistic for a pre-established level of significant (typically $p < 0.05$) can lead to the rejection of the null hypothesis, meaning that the data were not likely to have been sampled from populations with the same mean.

3.5. Experimental Design and Optimization

3.5.1. Preliminary Experiments

Experiments and optimization were performed in three stages. In the first stage, preliminary experiments were conducted to determine the ranges of experimental factors to be used in the main experiments. In the second stage, the main experiments were conducted to determine optimal experimental conditions using the response surface methodology. Finally, in the third stage, reaction kinetics were investigated under optimized operational conditions.

Four independent factors including pH, initial dye concentration, TiO_2 dose and reaction time were used to evaluate dye removal efficiencies in the preliminary first-stage experiments. Adopting a one factor-at-a-time approach, three out of four variables were held constant and the fourth was varied in 4 or 5 levels. Table 6 shows variables and levels used in the preliminary experiments. Two replicate runs were conducted for each combination.

Table 6. Experimental factors and levels used in preliminary experiments for photocatalytic degradation of AB 113 and AR 88 in the UV-C/TiO_2 system.

Variables	Levels				
pH	2.0	3.0 *	6.0	9.0	10.0
Initial dye concentration (mg/L)	20	50 *	100	150	200
TiO_2 dose (g/L)	0.5	1.0 *	2.0	4.0	-
Reaction time (min)	30	60	90 *	120	180

* Fixed value of variable when other factors changed.

3.5.2. Experimental Design Using Response Surface Methodology

Experimental design, statistical analyses, mathematical modeling and optimizations were accomplished using Design Expert software (Design-Expert®, V 10, Stat-Ease, Inc., Minneapolis, MN, USA). Similar to the paper by Saber et al. [26], a cubic IV optimal design method was employed to investigate the effects of input factors and their interactions on dye removal percentage (i.e., the target response), in the second experimental stage. Cubic IV optimal design minimizes the integral of prediction variance through the design space and results in a lower prediction variance throughout an area of interest [59]. Ranges of experimental variables were considered based on the results from preliminary experiments. As Table 7 shows, six levels of pH, six levels of TiO_2 dose and six levels of initial dye concentration were considered as the independent variables in the optimal design. For each

dye, 30 combinations of conditions were developed according to the cubic IV optimal design algorithm. The achieved removal efficiency for each run was considered as the target response. In order to account for experimental errors, three replicate runs were conducted for each combination of conditions and the average removal efficiency of the three runs was reported for each experimental run.

Table 7. Experimental factors and their levels used in cubic IV optimal design for photocatalytic degradation of AB 113 and AR 88.

Factors	Levels					
A: pH	2.0	2.5	3.0	3.5	4.0	5.0
B: TiO_2 dose (g/L)	0.5	1.0	1.5	2.0	2.5	3.0
C: Initial dye concentration (mg/L)	20	50	60	80	115	150

Analysis of variance (ANOVA) was performed on the fitted cubic models for each dye to evaluate the significance of the fitted models and to identify the relative significance of experimental factors and their interactions on the removal efficiency for each dye. Three-dimensional response surface and contour plots were generated based on the cubic least-squares regression models obtained from ANOVA.

3.5.3. Kinetic Studies

In the third stage, additional experiments were conducted to investigate reaction kinetics under the optimized treatment conditions determined from the cubic IV optimal experimental design.

A first-order kinetic model can be described as:

$$\ln(C) = \ln(C_o) - k_1 t \tag{15}$$

where, t is the reaction time (min), C_o and C (mg/L) are the initial dye concentration (mg/L) and dye concentration at time t, respectively and k_1 is the first-order reaction rate constant (min^{-1}). When evaluating goodness of fit for a kinetic model, root mean square error (*RMSE*) (Equation (16)) was used along with R^2 value to evaluate model validity [60].

$$RMSE = \sqrt{\frac{\sum_{i=1}^{n}\left(C_m - C_{exp}\right)^2}{n}} \tag{16}$$

where C_{exp} and C_m are the experimental and calculated values (based on the fitted kinetic models) of dye concentration and n is the number of data points.

4. Conclusions

This study optimized photodegradation of AB 113 and AR 88 dyes in a UV-C/TiO_2 suspension system using RSM, considering initial dye concentration, solution pH and catalyst dose as variant factors and the removal percentage as the target response. Under optimum conditions, kinetics of photocatalytic degradation of AB 113 and AR 88 were also investigated. Analysis of variance showed that reduced cubic models could well describe the removal of AB 113 and AR 88 dyes. The F-test showed that the solution pH and initial dye concentration were the most important parameters for removal of AB 113 and AR 88, respectively. Although pH was the most significant parameter affecting AB 113 removal efficiency, it was found to be insignificant for AR 88 removal. However, pH of the AR 88 solution showed significant interactions with the other two factors. Degradation efficiencies of 98.7% and 99.6% were achieved under optimum conditions for AB 113 and AR 88, respectively. The present study demonstrated almost complete degradation of AB 113 and AR 88 in 90 min under the optimized conditions obtained using RSM, with first-order rate constants of degradation rate constants of $k_{1,\,AB\,113} = 0.048\ min^{-1}$ and $k_{1,\,AR\,88} = 0.059\ min^{-1}$.

Results show that a UV-C/TiO_2 photocatalytic degradation process can be considered as a promising and cost-effective technique for dye removal from textile industry effluents. As a proposal, a dyeing plant could adjust conditions in its effluent to the optimized values to obtain more than 98.7% destruction of waste dye and then adjust effluent pH to neutral values and filter to remove and recycle the TiO_2 particles prior to discharge to a receiving water. Additional batch experiments should be conducted at a bench scale in multi dye solutions to evaluate competition between various dyes, followed by pilot-scale application of this treatment method on a real textile wastewater in a flow-through reactor to evaluate limitations due to incomplete mixing and dispersion.

Supplementary Materials: The following are available online at http://www.mdpi.com/2073-4344/9/4/360/s1, Figure S1: Computed F-values for significant ($p < 0.05$) regression model terms associated with photocatalytic degradation of (a) AB 113 (a) and (b) AR 88 [*A*: pH, *B*: TiO_2 dose (g/L) and *C*: Initial dye concentration: (mg/L)]., Figure S2: Absorbance versus dye concentrations graphs for (a) AB 113 and (b) AR 88, showing linearity of data for both dyes in the studied dye concentration between 0 mg/L to 200 mg/L.

Author Contributions: Conceptualization, S.M. and A.S.; Data curation, S.M. and A.S.; Formal analysis, S.M., A.S. and D.E.J.; Funding acquisition, D.E.J.; Investigation, S.M.; Methodology, S.M. and A.S.; Software, S.M. and A.S.; Supervision, D.E.J.; Validation, S.M. and A.S.; Visualization, S.M.; Writing—original draft, S.M.; Writing—review & editing, A.S. and D.E.J.

Funding: The publication fees for this article were supported by the UNLV University Libraries Open Article Fund. Authors thank Isfahan University of Technology for partially funding (1391-7) this research.

Acknowledgments: Authors would like to acknowledge Amir Taebi for his professional advice and Behnaz Harandizadeh for her help in running experiments. The authors greatly appreciate the anonymous reviewers of this manuscript for their constructive suggestions which improved the quality of this study.

Conflicts of Interest: The authors declare no conflict of interest.

References

1. Sohrabi, M.R.; Ghavami, M. Photocatalytic degradation of Direct Red 23 dye using UV/TiO_2: Effect of operational parameters. *J. Hazard. Mater.* **2008**, *153*, 1235–1239. [CrossRef]
2. Houas, A.; Lachheb, H.; Ksibi, M.; Elaloui, E.; Guillard, C.; Herrmann, J.-M. Photocatalytic degradation pathway of methylene blue in water. *Appl. Catal. B Environ.* **2001**, *31*, 145–157. Available online: https://ac-els-cdn-com.ezproxy.library.unlv.edu/S0926337300002769/1-s2.0-S0926337300002769-main.pdf?_tid=7e7afe96-d229-11e7-85a6-00000aab0f26&acdnat=1511646312_3be9e82c1ae096d6f42aa8199f88814d (accessed on 25 November 2017). [CrossRef]
3. Konicki, W.; Sibera, D.; Mijowska, E.; Lendzion-Bieluń, Z.; Narkiewicz, U. Equilibrium and kinetic studies on acid dye Acid Red 88 adsorption by magnetic ZnFe2O4 spinel ferrite nanoparticles. *J. Colloid Interface Sci.* **2013**, *398*, 152–160. [CrossRef] [PubMed]
4. Gupta, A.K.; Pal, A.; Sahoo, C. Photocatalytic degradation of a mixture of Crystal Violet (Basic Violet 3) and Methyl Red dye in aqueous suspensions using Ag+ doped TiO_2. *Dyes Pigments* **2006**, *69*, 224–232. [CrossRef]
5. Han, F.; Kambala, V.S.R.; Srinivasan, M.; Rajarathnam, D.; Naidu, R. Tailored titanium dioxide photocatalysts for the degradation of organic dyes in wastewater treatment: A review. *Appl. Catal. A Gen.* **2009**, *359*, 25–40. [CrossRef]
6. Konstantinou, I.K.; Albanis, T.A. TiO_2-assisted photocatalytic degradation of azo dyes in aqueous solution: Kinetic and mechanistic investigations: A review. *Appl. Catal. B Environ.* **2004**, *49*, 1–14. [CrossRef]
7. Juang, R.S.; Lin, S.H.; Hsueh, P.Y. Removal of binary azo dyes from water by UV-irradiated degradation in TiO_2 suspensions. *J. Hazard. Mater.* **2010**, *182*, 820–826. [CrossRef]
8. Ahmed, S.; Rasul, M.G.; Martens, W.N.; Brown, R.; Hashib, M.A. Heterogeneous photocatalytic degradation of phenols in wastewater: A review on current status and developments. *Desalination* **2010**, *261*, 3–18. [CrossRef]
9. Barakat, M.A. Adsorption and photodegradation of Procion yellow H-EXL dye in textile wastewater over TiO_2 suspension. *J. Hydro-Environ. Res.* **2011**, *5*, 137–142. [CrossRef]
10. Soutsas, K.; Karayannis, V.; Poulios, I.; Riga, A.; Ntampegliotis, K.; Spiliotis, X.; Papapolymerou, G. Decolorization and degradation of reactive azo dyes via heterogeneous photocatalytic processes. *Desalination* **2010**, *250*, 345–350. [CrossRef]

11. Anandan, S.; Kumar, P.S.; Pugazhenthiran, N.; Madhavan, J.; Maruthamuthu, P. Effect of loaded silver nanoparticles on TiO_2 for photocatalytic degradation of Acid Red 88. *Sol. Energy Mater. Sol. Cells* **2008**, *92*, 929–937. [CrossRef]
12. Zayani, G.; Bousselmi, L.; Pichat, P.; Mhenni, F. Photocatalytic degradation of the Acid Blue 113 textile azo dye in aqueous suspensions of four commercialized TiO(2) samples. *J. Environ. Sci. Health A Tox. Hazard. Subst. Environ. Eng.* **2008**, *43*, 202–209. [CrossRef]
13. Gupta, V.K.; Jain, R.; Mittal, A.; Saleh, T.A.; Nayak, A.; Agarwal, S.; Sikarwar, S. Photo-catalytic degradation of toxic dye amaranth on TiO_2/UV in aqueous suspensions. *Mater. Sci. Eng. C* **2012**, *32*, 12–17. [CrossRef] [PubMed]
14. Toor, A.T.; Verma, A.; Jotshi, C.K.; Bajpai, P.K.; Singh, V. Photocatalytic degradation of Direct Yellow 12 dye using UV/TiO_2 in a shallow pond slurry reactor. *Dyes Pigments* **2006**, *68*, 53–60. [CrossRef]
15. Khataee, A.R.; Pons, M.N.; Zahraa, O. Photocatalytic degradation of three azo dyes using immobilized TiO_2 nanoparticles on glass plates activated by UV light irradiation: Influence of dye molecular structure. *J. Hazard. Mater.* **2009**, *168*, 451–457. [CrossRef] [PubMed]
16. Balachandran, K.; Venckatesh, R.; Sivaraj, R.; Rajiv, P. TiO_2 nanoparticles versus TiO_2-SiO_2 nanocomposites: A comparative study of photo catalysis on acid red 88, Spectrochim. *Acta Part A Mol. Biomol. Spectrosc.* **2014**, *128*, 468–474. [CrossRef] [PubMed]
17. Gao, B.; Yap, P.S.; Lim, T.M.; Lim, T.T. Adsorption-photocatalytic degradation of Acid Red 88 by supported TiO_2: Effect of activated carbon support and aqueous anions. *Chem. Eng. J.* **2011**, *171*, 1098–1107. [CrossRef]
18. Moon, J.; Yun, C.Y.; Chung, K.W.; Kang, M.S.; Yi, J. Photocatalytic activation of TiO_2 under visible light using Acid Red 44. *Catal. Today* **2003**, *87*, 77–86. [CrossRef]
19. Khataee, A.R.; Zarei, M. Photoelectrocatalytic decolorization of diazo dye by zinc oxide nanophotocatalyst and carbon nanotube based cathode: Determination of the degradation products. *Desalination* **2011**, *278*, 117–125. [CrossRef]
20. Cavazzuti, M. *Optimization Methods: From Theory to Design Scientific and Technological Aspects in Mechanics*; Springer: New York, NY, USA, 2013. [CrossRef]
21. Antony, J. Taguchi or classical design of experiments: A perspective from a practitioner. *Sens. Rev.* **2006**, *26*, 227–230. [CrossRef]
22. Khuri, A.I.; Mukhopadhyay, S. Response surface methodology, Wiley Interdiscip. *Rev. Comput. Stat.* **2010**, *2*, 128–149. [CrossRef]
23. Myers, R.H.; Montgomery, D.C.; Anderson-Cook, C.M. *Response Surface Methodology: Process and Product Optimization Using Designed Experiments*, 3rd ed.; John Wiley & Sons: New York, NY, USA, 2009.
24. Wei, L.; Zhu, H.; Mao, X.; Gan, F. Electrochemical oxidation process combined with UV photolysis for the mineralization of nitrophenol in saline wastewater. *Sep. Purif. Technol.* **2011**, *77*, 18–25. [CrossRef]
25. Sahu, J.N.; Acharya, J.; Meikap, B.C. Response surface modeling and optimization of chromium(VI) removal from aqueous solution using Tamarind wood activated carbon in batch process. *J. Hazard. Mater.* **2009**, *172*, 818–825. [CrossRef] [PubMed]
26. Saber, A.; Mortazavian, S.; James, D.E.; Hasheminejad, H. Optimization of Collaborative Photo-Fenton Oxidation and Coagulation for the Treatment of Petroleum Refinery Wastewater with Scrap Iron. *Water Air Soil Pollut.* **2017**, *228*. [CrossRef]
27. Saber, A.; Hasheminejad, H.; Taebi, A.; Ghaffari, G. Optimization of Fenton-based treatment of petroleum refinery wastewater with scrap iron using response surface methodology. *Appl. Water Sci.* **2014**, *4*, 283–290. [CrossRef]
28. Zhu, X.; Tian, J.; Liu, R.; Chen, L. Optimization of fenton and electro-fenton oxidation of biologically treated coking wastewater using response surface methodology. *Sep. Purif. Technol.* **2011**, *81*, 444–450. [CrossRef]
29. Benatti, C.T.; Tavares, C.R.G.; Guedes, T.A. Optimization of Fenton's oxidation of chemical laboratory wastewaters using the response surface methodology. *J. Environ. Manag.* **2006**, *80*, 66–74. [CrossRef] [PubMed]
30. Ahmadi, M.; Vahabzadeh, F.; Bonakdarpour, B.; Mofarrah, E.; Mehranian, M. Application of the central composite design and response surface methodology to the advanced treatment of olive oil processing wastewater using Fenton's peroxidation. *J. Hazard. Mater.* **2005**, *123*, 187–195. [CrossRef]
31. Bianco, B.; de Michelis, I.; Vegliò, F. Fenton treatment of complex industrial wastewater: Optimization of process conditions by surface response method. *J. Hazard. Mater.* **2011**, *186*, 1733–1738. [CrossRef] [PubMed]

32. Bagheri, A.R.; Ghaedi, M.; Asfaram, A.; Bazrafshan, A.A.; Jannesar, R. Comparative study on ultrasonic assisted adsorption of dyes from single system onto Fe_3O_4 magnetite nanoparticles loaded on activated carbon: Experimental design methodology. *Ultrason. Sonochem.* **2017**, *34*, 294–304. [CrossRef] [PubMed]
33. Mohajeri, S.; Aziz, H.A.; Isa, M.H.; Zahed, M.A.; Adlan, M.N. Statistical optimization of process parameters for landfill leachate treatment using electro-Fenton technique. *J. Hazard. Mater.* **2010**, *176*, 749–758. [CrossRef] [PubMed]
34. Cifuentes, B.; Figueredo, M.; Cobo, M. Response Surface Methodology and Aspen Plus Integration for the Simulation of the Catalytic Steam Reforming of Ethanol. *Catalysts* **2017**, *7*, 15. [CrossRef]
35. Li, L.; Ma, Q.; Wang, S.; Song, S.; Li, B.; Guo, R.; Cheng, X.; Cheng, Q. Photocatalytic Performance and Degradation Mechanism of Aspirin by TiO_2 through Response Surface Methodology. *Catalysts* **2018**, *8*, 118. [CrossRef]
36. Inger, M.; Dobrzyńska-Inger, A.; Rajewski, J.; Wilk, M. Optimization of Ammonia Oxidation Using Response Surface Methodology. *Catalysts* **2019**, *9*, 249. [CrossRef]
37. Aljuboury, D.a.A.; Palaniandy, P.; Aziz, H.B.A.; Feroz, S.; Amr, S.S.A. Evaluating photo-degradation of COD and TOC in petroleum refinery wastewater by using TiO_2/ZnO photo-catalyst. *Water Sci. Technol.* **2016**, *74*, 1312–1325. [CrossRef]
38. Mohammadzadeh, S.; Olya, M.E.; Arabi, A.M.; Shariati, A.; Nikou, M.R.K. Synthesis, characterization and application of ZnO-Ag as a nanophotocatalyst for organic compounds degradation, mechanism and economic study. *J. Environ. Sci.* **2015**, *35*, 194–207. [CrossRef] [PubMed]
39. Mohan, D.; Pittman, C.U. Activated carbons and low cost adsorbents for remediation of tri- and hexavalent chromium from water. *J. Hazard. Mater.* **2006**, *137*, 762–811. [CrossRef]
40. Alkaim, A.F.; Kandiel, T.A.; Hussein, F.H.; Dillert, R.; Bahnemann, D.W. Enhancing the photocatalytic activity of TiO_2 by pH control: A case study for the degradation of EDTA. *Catal. Sci. Technol.* **2013**, *3*, 3216. [CrossRef]
41. Hu, C.; Yu, J.C.; Hao, Z.; Wong, P.K. Effects of acidity and inorganic ions on the photocatalytic degradation of different azo dyes. *Appl. Catal. B Environ.* **2003**, *46*, 35–47. [CrossRef]
42. Shirzad-Siboni, M.; Jafari, S.J.; Giahi, O.; Kim, I.; Lee, S.M.; Yang, J.K. Removal of acid blue 113 and reactive black 5 dye from aqueous solutions by activated red mud. *J. Ind. Eng. Chem.* **2014**, *20*, 1432–1437. [CrossRef]
43. Lima, E.C.; Royer, B.; Vaghetti, J.C.P.; Simon, N.M.; da Cunha, B.M.; Pavan, F.A.; Benvenutti, E.V.; Cataluña-Veses, R.; Airoldi, C. Application of Brazilian pine-fruit shell as a biosorbent to removal of reactive red 194 textile dye from aqueous solution. Kinetics and equilibrium study. *J. Hazard. Mater.* **2008**, *155*, 536–550. [CrossRef] [PubMed]
44. Habibi, M.H.; Vosooghian, H. Photocatalytic degradation of some organic sulfides as environmental pollutants using titanium dioxide suspension. *J. Photochem. Photobiol. A Chem.* **2005**, *174*, 45–52. [CrossRef]
45. Venkatachalam, N.; Palanichamy, M.; Murugesan, V. Sol-gel preparation and characterization of alkaline earth metal doped nano TiO_2: Efficient photocatalytic degradation of 4-chlorophenol. *J. Mol. Catal. A Chem.* **2007**, *273*, 177–185. [CrossRef]
46. Fox, M.A.; Dulay, M.T. Heterogeneous photocatalysis. *Chem. Rev.* **1993**, *93*, 341–357. [CrossRef]
47. Ma, C.-M.; Hong, G.-B.; Chen, H.-W.; Hang, N.-T.; Shen, Y.-S. Photooxidation Contribution Study on the Decomposition of Azo Dyes in Aqueous Solutions by VUV-Based AOPs. *Int. J. Photoenergy* **2011**, *2011*, 1–8. [CrossRef]
48. Saharan, V.K.; Pandit, A.B.; Kumar, P.S.S.; Anandan, S. Hydrodynamic cavitation as an advanced oxidation technique for the degradation of Acid Red 88 dye. *Ind. Eng. Chem. Res.* **2012**, *51*, 1981–1989. [CrossRef]
49. Spiess, A.N. qpcR package V1.4-0, Modeling and Analysis of Real-Time PCR Data. 2018. Available online: https://www.rdocumentation.org/packages/qpcR/versions/1.4-0 (accessed on 31 May 2018).
50. Konyar, M.; Yildiz, T.; Aksoy, M.; Yatmaz, H.C.; Öztürk, K. Reticulated *ZnO* Photocatalyst: Efficiency Enhancement in Degradation of Acid Red 88 Azo Dye by Catalyst Surface Cleaning. *Chem. Eng. Commun.* **2017**, *204*, 711–716. [CrossRef]
51. Camarillo, R.; Rincón, J. Photocatalytic Discoloration of Dyes: Relation between Effect of Operating Parameters and Dye Structure. *Chem. Eng. Technol.* **2011**, *34*, 1675–1684. [CrossRef]
52. Stylidi, M.; Kondarides, D.I.; Verykios, X.E. Visible light-induced photocatalytic degradation of Acid Orange 7 in aqueous TiO_2 suspensions. *Appl. Catal. B Environ.* **2004**, *47*, 189–201. [CrossRef]
53. Madhavan, J.; Kumar, P.S.S.; Anandan, S.; Grieser, F.; Ashokkumar, M. Degradation of acid red 88 by the combination of sonolysis and photocatalysis. *Sep. Purif. Technol.* **2010**, *74*, 336–341. [CrossRef]

54. Trotma, E.R. *Dyeing and Chemical Technology of Textile Fibres*; Griffin: London, UK, 1970; Available online: https://www.scribd.com/doc/101550453/Dyeing-and-Chemical-Technology-of-Textile-Fibres (accessed on 3 May 2017).
55. Martínez-Huitle, C.A.; Brillas, E. Decontamination of wastewaters containing synthetic organic dyes by electrochemical methods: A general review. *Appl. Catal. B Environ.* **2009**, *87*, 105–145. [CrossRef]
56. Shu, H.Y.; Chang, M.C.; Chen, C.C.; Chen, P.E. Using resin supported nano zero-valent iron particles for decoloration of Acid Blue 113 azo dye solution. *J. Hazard. Mater.* **2010**, *184*, 499–505. [CrossRef] [PubMed]
57. Meyers, R. *Encyclopedia of Physical Science and Technology*; Academic Press: New York, NY, USA, 2002.
58. Zumel, N. Estimating Generalization Error with the PRESS statistic|Win-Vector Blog, (2014) 12. Available online: http://www.win-vector.com/blog/2014/09/estimating-generalization-error-with-the-press-statistic/ (accessed on 2 April 2019).
59. Anderson, M.J.; Whitcomb, P.J. *RSM Simplified: Optimizing Processes Using Response Surface Methods for Design of Experiments*; Productivity Press: New York, NY, USA, 2005. Available online: https://www.crcpress.com/RSM-Simplified-Optimizing-Processes-Using-Response-Surface-Methods-for/Whitcomb-Anderson/p/book/9781563272974 (accessed on 3 May 2017).
60. Saber, A.; Tafazzoli, M.; Mortazavian, S.; James, D.E. Investigation of kinetics and absorption isotherm models for hydroponic phytoremediation of waters contaminated with sulfate. *J. Environ. Manag.* **2018**, *207*, 276–291. [CrossRef] [PubMed]